Similar progression of morphological and metabolic phenotype in R6/2 mice with different CAG repeats revealed by *in vivo* magnetic resonance imaging and spectroscopy

Stephen J Sawiak[a, b, 1], Nigel I Wood[c, 1] and A Jennifer Morton[c]

[a]Wolfson Brain Imaging Centre, University of Cambridge, Box 65 Addenbrooke's Hospital, Hills Road, Cambridge, CB2 0QQ

[b]Behavioural and Clinical Neuroscience Institute, University of Cambridge, Downing Street, Cambridge CB2 3EB

[c]Physiology, Development and Neuroscience, University of Cambridge, Downing Street, Cambridge CB2 3DY

Author for correspondence:

Professor Jenny Morton
Department of Physiology, Development and Neuroscience
University of Cambridge
Downing Street
Cambridge CB2 3DY
UNITED KINGDOM

Tel +44 1223 334057

Fax +44 1223 333840

E-mail: ajm41@cam.ac.uk

[1]The authors wish it to be known that the first two authors should be regarded as joint First Authors.

Running title: CAG repeat-dependent MRI/MRS changes in R6/2 mice

Abstract

Background: Huntington's disease (HD) is caused by an unstable polyglutamine (CAG) repeat in the HD gene, whereby a CAG repeat length greater than ~36 leads to the disease. In HD patients, longer repeats correlate with more severe disease and earlier death. This is also seen in R6/2 mice carrying repeat lengths up to ~200. Paradoxically, R6/2 mice with repeat lengths >300 have a less aggressive phenotype and longer lifespan than those with shorter repeats. The mechanism underlying this phenomenon is unknown.

Objective: To investigate the consequences of longer repeat lengths on structural changes in the brains of R6/2 mice, especially with regard to progressive atrophy.

Methods: We used longitudinal *in vivo* magnetic resonance imaging (MRI) and spectroscopy (MRS) to compare pathological changes in two strains of R6/2 mice, one with a rapidly progressing disease (250 CAG repeats), and the other with a less aggressive phenotype (350 CAG repeats).

Results: We found significant progressive brain atrophy in both 250 and 350 CAG repeat mice, as well as changes in metabolites (glutamine/glutamate, choline and aspartate). Although similar in magnitude, atrophy in the brains of 350 CAG R6/2 mice progressed more slowly than that seen in 250 CAG mice, in line with the milder phenotype and longer lifespan. Interestingly, significant atrophy was detectable in 350 CAG mice as early as 8-12 weeks of age, although behavioural abnormalities in these mice are not apparent before 25-30 weeks. This finding fits well with human data from the PREDICT-HD and TRACK-HD project, where reductions in brain volume were found 10 years in advance of the onset of symptoms.

Conclusions: The similar brain atrophy with a mismatch between onset of brain atrophy and behavioural phenotype in HD mice with 350 repeats will make this mouse particularly useful for modelling early stages of HD pathology.

Keywords: MRI; MRS; tensor-based morphometry; neurodegenerative disease; trinucleotide repeat disorders

Introduction

Huntington's disease is a fatal, progressive neurodegenerative disorder caused by an unstable polyglutamine (CAG) expansion in the gene coding for the protein huntingtin. It is characterised by motor dysfunction, notably chorea, as well as cognitive, psychiatric and sleep abnormalities. Death typically occurs 12-15 years from the first symptoms [1]. HD pathology is characterised by striatal and cortical neurodegeneration that is accompanied by the presence of aggregates of mutant huntingtin. These aggregates have been found in the nucleus and cytoplasm of both humans [2] and mouse models of HD [3, 4]. The precise role of the inclusions in disease development has yet to be resolved.

The expanded CAG repeat that causes HD is inherently unstable. In both HD patients and mouse models, somatic variation in CAG repeat number affects both age at onset and severity of the disease symptoms. An expansion of 35-37 CAG repeats is sufficient to cause HD [5], and longer repeats correlate with earlier age at onset of symptoms [6]. However, variability in age of onset is only partly explained by the number of CAG repeats, indicating that other factors are involved [7]. It has been suggested that in HD patients' brains, somatic CAG repeat expansion occurs until the repeat length reaches a pathological threshold [8]. Therefore, the age of onset of HD is dependent upon both the initial length of the CAG repeat, and the time it takes for the unstable expansions to reach the toxic threshold. This fits with evidence from studies showing that individuals carrying HD gene mutations are overtly neurologically normal until phenoconversion [9, 10]. Even so, results from the PREDICT-HD and TRACK-HD initiative show that brain volume loss can be detected up to 10 years before symptoms become manifest, suggesting a long-term, insidious, process of neuronal loss that only gradually produces any clinical signs

[11-14]. However, evidence is accumulating to show that subtle cognitive impairment may also be present in HD patients for some years before diagnosis, suggesting that the mismatch between onset of brain changes and detection of symptoms may be partly due to incomplete diagnostic criteria [15-17].

Most mouse models of HD have, by comparison with humans, very long CAG repeat lengths (typically in the range 110-250). This is well-recognised in the field to be a caveat to the appropriateness of the models. However, the need for greater initial repeat lengths in mice may be explained by the Kaplan model [8], which predicts that unstable expansions need to reach a toxic threshold of ~115 CAGs before pathology is seen. The life span of a mouse (approximately 2 years) may be insufficient to allow a pathology-inducing expansion to be reached from a short inherited CAG repeat length in the range that causes disease in humans.

We have previously reported that there are considerable age differences in the onset of abnormal phenotype in the R6/2 transgenic mouse model of HD, with the relationship between age and CAG repeat length being U-shaped. As the number of CAG repeats increases past 200, so does life span [18]. Furthermore, the timing of appearance of the classically described neuronal intranuclear inclusions (NII) [19] is delayed in mice with >300 CAG repeats [18]. These findings were similar to those of Dragatsis and colleagues, who found an extended lifespan in mice carrying 300-400 repeats [20]. The idea that longer CAG repeats cause disease with a slower trajectory has also been supported by electrophysiological studies [21].

We were interested in investigating the consequences of longer repeat lengths on structural changes in the brains of R6/2 mice, especially with regard to the progressive atrophy that characterises HD. We used a mixed longitudinal and cross-

sectional experimental design to compare structural and biochemical changes in lines of R6/2 mice carrying 250 or 350 CAG repeats using *in vivo* high-resolution magnetic resonance imaging (MRI) and spectroscopy (MRS). The advantage of this non-invasive method is that a detailed trajectory of morphological changes can be monitored longitudinally without the need to sacrifice large numbers of animals at each time point. Automated voxel-based morphometry has proved a sensitive method for identifying morphological differences in mouse models of HD both *in vivo* [22] and *ex vivo* [23].

Materials and Methods

Mice

All procedures were conducted in accordance with the UK Animals (Scientific Procedures) Act 1986, and were approved by the University of Cambridge Animal Welfare and Ethical Review Board.

Mice were taken from colonies of R6/2 mice established in the University of Cambridge, and maintained by backcrossing onto CBA x C57BL6 F1 female mice. Methods for the genotyping of these mice, and details of the animal husbandry, have been described previously [3, 24]. Briefly, mice were housed in single-sex, single-genotype groups of 3-4 at 21-23°C with humidity of 55 ± 10%. Lowered waterspouts were provided for *ad libitum* access to water and standard dry laboratory food was given. A supplementary feed (of mash made by soaking 100g dry food in 230 ml of filtered tap water until pellets were soft and fully expanded) was given each morning and evening. Enrichment was provided by the addition of plastic houses, cardboard tubes and chew blocks to the cages. Genotyping and CAG repeat length measurement were carried out by Laragen (Los Angeles, CA, USA). We selected

two groups of transgenic mice (hereafter called 250 CAG and 350 CAG), with CAG repeat lengths of either 253 ± 2 (mean ± SEM) or 354 ±3 respectively, as determined by GeneMapper.

We used 26 R6/2 250 CAG mice and 25 R6/2 350 CAG mice, with 35 age-matched wildtype (WT) mice as control mice. Scanning took place at 3 week intervals, when the mice were aged between 8-21 weeks (250 CAG), or 8-33 weeks (350 CAG). At each time point, scanning the entire cohort of mice took approximately 3 weeks, so data were collated in ~3 week blocks (8-12, 12-15, 15-18, 18-21, 21-24, 24-27, 27-30, 30-33 weeks).

Image acquisition

Mice were anaesthetised with isoflurane (1-2% in 1l/min O_2). Respiration rates were measured using a pressure-sensor (SA Instruments, Stony Brook, NY, USA). Depth of anaesthesia was adjusted according to the respiration rate to maintain a consistent level between mice. Body temperature was measured with a rectal probe and maintained in the normal range using a heated flowing-water blanket.

Structural Imaging

Mice were scanned at 4.7T using a Bruker BioSpec 47/40 system (Bruker Inc., Ettlingen, Germany). An actively-decoupled birdcage transmitter (model T5346) was used for excitation, and the manufacturer-provided quadrature mouse head surface coil (model T9788) was used for signal reception. Structural imaging was achieved with a rapid acquisition with relaxation enhancement (RARE) sequence (scan parameters: repetition time 3.5s, effective echo time 32ms, bandwidth 40 kHz, echo train length 12, field of view 25.6×19.2×10.0mm^3, matrix 256×192×100). The final resolution was 100μm isotropic, and images were acquired in 1 hour 33 minutes.

Magnetic resonance spectroscopy

Following structural imaging, a point-resolved selective spectroscopy (PRESS) voxel was positioned at the level of the left caudate putamen. The voxel extended 2mm in each direction (8µl) and was acquired with 128 transients with a repetition time of 2.5s and echo time 20ms. Water suppression was achieved with the variable power and optimized relaxation (VAPOR) scheme with manually-adjusted pulse power and localised shimming was performed using the manufacturer-provided FASTMAP routine with a 4mm cubic voxel centred on the smaller PRESS region. Outer volume suppression was enabled and a navigator signal was acquired for retrospective frequency locking.

MR data analysis

Tensor-based morphometry

Tensor-based morphometry (TBM) was performed using SPM8 (Wellcome Trust Centre for Neuroimaging, UCL) with the DARTEL registration software [25] modified for mice using the SPMMouse toolbox.

Images were aligned manually with the mouse template created during our previous voxel-based morphometry study [26] and segmented using unified segmentation [27]. DARTEL was used with the settings we have described previously [22] to produce maps of local volume change (Jacobian determinants).

We used the maps in three different ways. Firstly, we compared separately the local volume differences from R6/2 250 CAG mice or R6/2 350 CAG mice with those of WT mice at the age of 12-15 weeks, and also compared male with female mice in all three groups. Determinant maps were smoothed by a 400µm isotropic Gaussian

smoothing kernel. To control for the type I errors expected due to multiple comparisons, a false-discovery rate of $q < 0.05$ was used [28]. This correction means one can expect that, on average, 5% of the findings reported as significant will be false positives. Secondly, for visual comparison, we produced maps showing the mean difference between the Jacobian determinant of WT and R6/2 mice of each genotype at 8-12 weeks and for each 3 week block thereafter, as long as at least 4 mice survived per group (until 21 weeks in 250 CAG mice and 33 weeks in 350 CAG mice). Thirdly, we extracted mean determinants within regions of interest (ROI) [29] for each mouse at each time point to compare trajectories of change over time for each genotype. We measured the caudate putamen, cerebral cortex, lateral ventricles, internal capsule, hippocampal formation and amygdaloid nucleus. To compare rates of change, linear regression lines were calculated using Matlab R2014 (MathWorks, Cambridge, MA, USA) and statistical significance of regression slopes was assessed using permutation testing, preserving animal age though randomly permuting genotype labels. We first looked for sex differences in rates of volume change of the localised structures, and where none were present, data from male and female mice were combined for further analysis as described above.

Spectroscopy analysis

Spectra were analysed using basis functions with LCModel version 6.3 [30] from 4.0-0.2ppm using the 200MHz gamma PRESS basis set. For more accurate measurements, we followed the guidelines of the software and measured the sum of glycerophosphocholine and phosphocholine (hereafter referred to as choline and abbreviated to cho), the sum of n-acetylaspartate and n-acetylaspartylglutatamate (hereafter referred to as aspartate, abbreviated to NAA), glutamate and glutamine (hereafter referred to as total glutamine-glutamate, abbreviated to Glx). In addition,

we measured the amino acid taurine. Metabolites were only considered for analysis where the standard deviation of modelling fits (Cramér-Rao lower bound) was lower than 20% in more than 90% of spectra acquired. For normalisation, metabolites were considered as ratios to the sum of creatine and phosphocreatine for each voxel. There is a caveat to our spectroscopy data, which is that the use of total creatine and phosphocreatine levels to normalise metabolite values could lead to confounded values if levels of creatine itself change. It is possible to use water levels as an alternative [31]. However, there is also a potential confound with this technique. Given the atrophy of the striatum, and the increased ventricular volume in the region of the ^{1}H-MRS voxel, it is possible that all metabolites would appear to be decreased in concentration as the visible water signal increases. Therefore, there are disadvantages to both techniques, so we chose the one that was less affected by physical changes in the brain.

Results

Life spans of R6/2 mice were similar to those of our previous reports, with R6/2 250 CAG mice reaching end stage at 22-26 weeks and R6/2 350 CAG mice reaching end stage at 30-33 weeks. A total of 148 scans were acquired (37 from R6/2 250 mice, 49 from R6/2 350 CAG mice and 62 from WT control mice). Figure 1 shows MR images of end-stage morphology for R6/2 250 (Figure 1D-F) and 350 (Figure 1G-I) CAG mice (25 and 32 weeks respectively), with a 40 week old WT mouse (Figure 1A-C) used for comparison. Inspection of the images shows that cortical atrophy is particularly apparent in the R6/2 250 CAG mice, especially in the frontal cortex. Both groups of R6/2 mice showed enlarged ventricles with reduced striatal volume compared to WT controls.

We used TBM to look for differences between the brains of male and female mice at 12-15 week. No significant sex differences were found, even when the threshold for statistical significance was raised to exploratory levels (controlling the false-discovery rate at $p < 0.25$; data not shown). Since there were no sex differences, we combined male and female data in further analyses. TBM analysis of brains of mice aged 12-15 weeks showed widespread reductions of volume in both lines of R6/2 mice compared to WT mice. R6/2 250 CAG mice showed more regions of significantly lower volume than were seen in R6/2 350 CAG mice (Figure 2).The changes were predominantly in grey matter structures in both groups of mice. In R6/2 250 CAG mice(Figure 2A), several of the basal ganglia were reduced in volume, with highly significant clusters seen in the caudate putamen and substantia nigra, although no changes were detected in lateral parts of the globus pallidus. The cortex was also widely affected, with the most significant effects being seen in the frontal cortex and parietal cortices, to a lesser extent the temporal cortex, and with some apparent sparing of superior aspects to the occipital cortex. The hippocampal formation, and in particular the dentate gyrus, was also reduced in volume. The central grey matter was also affected. The cerebellum showed reduced volume, in particular the fifth and sixth lobes, while the brain stem and medulla were largely spared (Figure 2A). At 12-15 weeks, atrophy in 350 CAG mice (Figure 2B) was less wide-spread than in the 250 CAG mice. Significant changes were seen mainly in the striatum, sensorimotor cortex, amygdala, and hippocampal formation. The differences in the hippocampus were focal, and centred on the CA2 subfield and dentate gyrus, compared to the more global changes seen in the hippocampal formation of 250 CAG mice.

Figure 3 shows the measured difference in local volume over time at each part in the brain in R6/2 mice relative to WT mice. For 250 CAG mice, the substantial reductions in brain volume seen at 8-12 weeks increased over time, with corresponding enlargement of the ventricles. Expansion of the lateral ventricles mirrored atrophy of the striatum. Interestingly, significant atrophy was also seen in 350 CAG mice at 8-12 weeks, even though their behavioural phenotype is not evident until 25-30 weeks of age. Volume changes in 350 CAG mice at all ages examined up to end stage were less severe than they were in 250 CAG mice. There appears to be a time lag of approximately 10 weeks between the timing of appearance of a similar level of volume reduction in 250 and 350 CAG mice. For an example, compare damage at 8-12 weeks in 250 CAG mice with that at 18-21 weeks in 350 CAG mice (Figure 3). Notably, brain atrophy in 350 CAG mice never reached the final level of severity that was seen in 250 CAG mice, although both 250 and 350 CAG mice all died prematurely of the disease. The use of TBM in this study enabled us to detect changes in tissues that are further from grey and white matter boundaries than would be possible using VBM alone as in our previous study [26]. TBM showed that atrophy in the R6/2 cortex is not generalised, but rather is more prominent within discrete layers of the cortex in R6/2 mice, with the peripheral layers being least affected (Figure 4).

Longitudinal ROI measurements

The analysis for sex differences showed a greater rate of volume increase in the lateral ventricles for CAG 350 female mice when compared to male mice ($p < 0.002$; Supplementary Figure 1). There were no other significant differences in the rate of change of structures by sex. Significant longitudinal atrophy ($p < 2\times10\text{-}5$) was seen

in the cortex (Figure 5A), caudate putamen (Figure 5B), amygdaloid nucleus (Figure 5D), hippocampal formation (Figure 5E) and cerebellum (Figure 5G) in both the 250 and 350 CAG repeat R6/2 mice. As expected, the lateral ventricles significantly increased in volume in all R6/2 mice ($p < 2\times10\text{-}5$, Figure 5C). The internal capsule was unaffected (Figure 5F). When comparing data between R6/2 lines, a significant difference in rate of overall atrophy was seen for the cortex ($p < 0.002$, Figure 5A), caudate ($p<1\times10^{-5}$, Figure 5B), amygdaloid nucleus ($p<2\times10^{-5}$, Figure 5D), hippocampal formation ($p < 1\times10^{-5}$, Figure 5E), and cerebellum ($p < 1\times10^{-5}$, Figure 5G), with atrophy in the 350 CAG mice being much slower. No significant changes were seen in the internal capsule ($p = 0.3$, Figure 5F).

Metabolites

We measured the levels of four metabolites (NAA, Glx, cho, taurine), all of which showed age-dependent changes in one or both lines of R6/2 mice. Levels of the neuronal marker NAA decreased significantly with age in both R6/2 250 ($p < 0.0002$) and 350 CAG mice ($p<0.01$) when compared to WT mice (Figure 6A). Glx concentrations decreased with age faster in R6/2 than WT mice (250 CAG, $p < 0.006$ and 350 CAG, $p < 0.002$, Figure 6C). Compared to WT mice, taurine increased significantly over time in both 250 and 350 CAG mice ($p < 0.01$ and $p < 0.04$ respectively, Figure 6D). Interestingly, a significant decrease in choline concentration ($p < 0.05$) was seen in the R6/2 350 CAG mice but not the 250 CAG mice (Figure 6B).Comparing the R6/2 250 CAG and 350 CAG mice directly, significant differences were seen only for choline ($p < 0.01$) (Figure 6B).

To summarise our results, the MRI data show that structural and biochemical aspects of the neurodegenerative phenotype are similar in mice with 250 and 350 CAG repeats. Atrophy begins in the frontal cortex, sensorimotor cortex, caudate and amygdaloid nucleus for both 250 and 350 CAG repeat mice, but progression of the atrophy is much slower in 350 CAG repeat mice. These findings are consistent with the slower progression of the behavioural phenotype and extended life span of CAG 350 mice compared to 250 CAG mice [18].

Discussion

The unfavourable prognosis in HD patients and animal models in relation to longer CAG repeat lengths is widely reported [6, 32, 33]. However, evidence is accumulating to indicate that this is not a straightforward relationship, and that mouse models of HD with CAG repeat lengths over 200 have an ameliorated phenotype compared to mice with fewer repeats [18, 20, 21]. In this study, we used high resolution MRI, MRS and automated whole brain analysis to examine the development of neuronal atrophy in R6/2 mice with markedly different CAG repeat lengths, duration of disease and behavioural phenotypes. We compared directly R6/2 mice with 250 CAG repeats (that has a rapidly progressing disease) and 350 CAG repeats (that has an ameliorated phenotype and longer lifespan [18]). We found widespread brain atrophy in R6/2 250 CAG mice from 8 weeks of age, approximately 4 weeks before overt physical signs but after cognitive [34] and electrophysiological [20] changes are detectable. In 350 CAG mice, atrophy was also detectable at 8-12 weeks of age. This was an interesting result, as it anticipates the behavioural phenotype by at least 15 weeks [18]. However, it fits well with clinical data showing brain volume loss in HD patients some years before the onset

of symptoms [11, 12]. By 30-33 weeks of age the atrophy in the brains of 350 CAG mice was widespread and substantial, although the rate of atrophy throughout the mice's lifespan was very much slower and did not reach the severity of that seen in 250 CAG mice, even when the mice were at the end-stage of their phenotype. The significance of this is not clear, although it makes it unlikely that brain atrophy is the cause of either behavioural changes or death in R6/2 mice. It is interesting to note that R6/2 mice with even longer repeat lengths (550 CAG) also show profound neuronal loss in the striatum and cortex, yet have a normal mouse lifespan (unpublished data, C. Kielar and A.J. Morton). Our data suggest that there is a similar morphological trajectory but a different time course underlying the atrophy in the 250 and 350 CAG R6/2 mice. That is, the disease begins in the same place and progresses similarly in the two lines of mice. Previous characterisations of allelic series of R6/2 mice carrying much longer CAG repeat lengths than those seen in typical HD patients have used histological assessment [18, 20] or electrophysiology [21]. Each of these studies found that the correlation of CAG repeat length with worsening disease trajectories is overturned after a critical value: at some point the mice carrying more polyglutamine repeats in their transgenic HD gene have an increased life span and show a delayed phenotype of HD-like symptoms. Our current data fit well with these previous studies. For completeness, it would have been interesting to look at mice with shorter CAG repeats (e.g. 110 CAGs). However, these mice have a very aggressive phenotype and very short lifespan, which makes longitudinal scanning with multiple anaesthesia sessions difficult.

We found no sex differences in rate of changes of brain structures in the 250 CAG mice, in accordance with our previous studies [22, 26, 29]. However, we did find that in the 350 CAG mice, lateral ventricles increased in size faster in female

than male TG mice. This may be another manifestation of the differences in time course of changes between the two strains, i.e. there may be sex differences in the 250 CAG mice but they are so short-lived that they did not show up on our analysis. It has been reported that there are sex differences in brain volumes in R6/2 mice with 210 CAG repeats [35]. The difference in results between our current study and that of Rattray et al. may be explained by differences in methodology –we used an automated analysis (TBM), while the Rattray study used manual volumetry. It is interesting to note that while we found no absolute differences in brain structures between male and female CAG 350 mice at the 12-15 week timepoint, we did detect differences between the sexes in the rate of change. This emphasises the value of a longitudinal analysis, which can detect changes that might otherwise be missed.

We have referred to the reduction in brain volumes we found in R6/2 mice as atrophy. However, it has been suggested that mutant huntingtin can also cause developmental dysfunction that contributes to neurodegeneration [36]. A study using BACHD mice has led to the proposition that HD pathology has two components, one developmental and the other resulting from the long-term toxic effects of mutant huntingtin [37]. While BACHD mice have a different genetic construct to R6/2 mice, we cannot rule out the possibility that at least some of the volume reduction we have observed is due to a developmental process.

Our MRS data showed progressive declines in NAA, glutamine/glutamate and an increase in taurine in both lines of R6/2 mice. As was seen with structural MRI, the rate of change was slower in 350 than 250 CAG mice. Decreased NAA has also been reported in HD patients [38-40], and140-150 CAG R6/2 mice [41, 42]. Since levels of NAA may reflect the functional status of neuronal mitochondria [43], the reduced levels of NAA we found in the R6/2 mice may reflect neuronal dysfunction.

Our findings of reduced glutamine/glutamate levels in both 250 and 350 CAG R6/2 mice reflect data from HD patients [44, 45], and are consistent with the reduced glutamatergic signalling and receptor binding seen in symptomatic animals and humans [46, 47]. Increased taurine levels have been reported previously in 150 CAG R6/2 mice [42], zQ175 knock-in mice [31], and the APP mouse model of Alzheimer's disease [48]. Taurine protects against oxidative stress in the 3-NP model of HD [49], is associated with apoptosis in brain tumours [50], and helps regulate brain volume [51, 52]. It is possible that the elevated levels seen in models of HD (including those used here) are a homeostatic response to the widespread apoptosis and atrophy resulting from the phenotype. The reduction in choline levels that we found in 350 CAG R6/2 mice reflects data from 200 CAG R6/2 mice [53] and from HD patients, where a decrease in choline has been reported in the frontal cortex and putamen [40, 54]). It has been suggested that cellular dysfunction preceding death may lead to reduced concentrations of choline [54]. This being the case, it is interesting that choline levels were lower in the 350 CAG but not the 250 CAG R6/2 mice. This may suggest a compensatory mechanism in the more severe form of the disease, or that the 250 CAG mice died before choline levels changed. Either way, it would be interesting to study this further.

Taken together, our data show that although the overall pattern of atrophy is similar in the two strains, the underlying pathology has an extended timecourse in 350 CAG mice, which may contribute to their longer lifespan. It has been proposed that the aggressive phenotype in R6/2 mice with shorter repeats may be due to accumulation of mutant protein in the nucleus, and that the larger protein made in mice with longer repeats may be too big to enter the nucleus, leading to an amelioration of the phenotype [20]. Unpublished work in 550 CAG mice (C. Kielar &

A.J. Morton) showed the presence of many large extranuclear inclusions but few neuronal inclusions in these mice, adding weight to the theory that mutant huntingtin produced by very long CAG repeats may not enter the nucleus. Cell death still occurs, however, suggesting that the mechanism of toxicity does not depend on the formation or nuclear localisation of neuronal inclusions. A second possible mechanism comes from the study by Duzdevich et al., who found that in 350 CAG repeat mice, the proportion of DNA molecules with unusual structures was approximately double that seen in 250 CAG mice [24]. They suggested that these abnormal structures found in DNA with very long CAG repeats may reduce transcription of the transgene [24]. It is possible, therefore, that as repeat lengths increase, production of mutant huntingtin decreases, leading to prolonged cell survival compared to cells containing DNA with shorter CAG repeats.

Our current study builds on our previous examination of *ex vivo* 18 week old R6/2 mice [26]. In this study we have greater sensitivity due to (a) improved *in vivo* contrast and preserved overall brain shape (without the damage or variability introduced by extraction of the brain from the skull and consequent loss of cerebrospinal fluid pressure *post mortem)* and (b) the fact that we used TBM as opposed to the voxel-based morphometry (VBM) we used in our previous work. The methodological advantage of TBM is that local volume changes are used to compare morphology, instead of modulated grey and white matter volume scores [27, 55]. This avoids potential errors that may be caused by changes in the chemical properties of tissues within each voxel. For example, changes in water content affect signal intensity. Local changes in water content, which can occur as a result of pathological processes, could lead to voxels that would be classified by VBM as white matter in WT brain to be misclassified as grey matter in a transgenic brain.

Furthermore, and importantly for small brains such as those of mice, TBM is more sensitive than VBM to changes that are further from grey and white matter boundaries. This increased sensitivity allowed us to identify atrophy within layers of the cortex in R6/2 mice, while our earlier VBM study restricted our findings to atrophy of the cortex as a whole [26].

Conclusion

We have compared, for the first time using *in vivo* longitudinal volumetric and spectroscopic measures, two allelic strains of R6/2 mice, one with 250 and one with 350 CAG repeats. Although the 350 CAG mice display a delayed and prolonged behavioural phenotype, and live longer than those mice with 250 CAG repeats, early atrophy was seen in the brains of these mice, with atrophy preceding behavioural changes by at least 10 weeks in the 350 CAG repeat mice. The pattern of progressive structural changes seen was similar in both lines of mice, with atrophy beginning in the frontal cortex, sensorimotor cortex and then progressing to other brain regions. MRS data also show a similar pattern of changes in 250 and 350 CAG mice, with reductions in levels of NAA and glutamine/glutamate and increases in taurine levels in both strains of transgenic mice. The slower MRI and MRS phenotype in mice with 350 CAG repeats confirms the toxicity mismatch, since the 350 CAG mice develop significant brain pathology in the absence of a behavioural phenotype. We suggest that the 350 CAG R6/2 mouse will be an excellent model for studying the expanded CAG repeat-dependent mechanisms of toxicity in HD. The similar but slower rate of disease progression and extended lifespan, relative to the

250 CAG mice, also provides a long window of opportunity in which to evaluate both pathological mechanisms and potential therapies.

Acknowledgements

We are grateful to Dr Adrian Carpenter for helpful discussions, and to Dr Desmond Tse, Karen Skelton, Dr Simon Puttick and Dr Guido Buonincontri for assistance with animal husbandry and acquisition of the MRI data.

This project was funded by a grant from CHDI *Inc*.

Conflict of interest

The authors have no conflict of interest to report.

References

[1] Walker FO. Huntington's disease. Lancet 2007; 369**:** 218-28.

[2] Sapp E, Schwarz C, Chase K, Bhide PG, Young AB, Penney J et al. Huntingtin localization in brains of normal and Huntington's disease patients. Ann Neurol. 1997; 42(4): 604-12.

[3] Morton AJ, Lagan MA, Skepper JN, Dunnett SB. Progressive formation of inclusions in the striatum and hippocampus of mice transgenic for the human Huntington's disease mutation. J. Neurocytol. 2000; 29**:** 679-702.

[4] Menalled LB, Chesselet MF. Mouse models of Huntington's disease. Trends Pharmacol. Sci. 2002; 23(1): 32-9.

[5] Rubinsztein DC, Leggo J, Coles R, Almqvist E, Biancalana V, Cassiman JJ et al. Phenotypic characterization of individuals with 30-40 CAG repeats in the Huntington disease (HD) gene reveals HD cases with 36 repeats and apparently normal elderly individuals with 36-39 repeats. Am. J. Hum. Genet. 1996; 59(1): 16-22.

[6] Orr HT, Zoghbi HY. Trinucleotide repeat disorders. Ann. Rev. Neurosci. 2007; 30**:** 575-621.

[7] Andresen JM, Gayán, J, Djoussé L, Roberts S, Brocklebank D, Cherny SS et al. The relationship between CAG repeat length and age of onset differs for Huntington's disease patients with juvenile onset or adult onset. Ann. Hum. Genet. 2007; 71(3): 295-301.

[8] Kaplan S, Itzkovitz S, Shapiro E. A universal mechanism ties genotype to phenotype in trinucleotide diseases. PLoS Comput. Biol. 2007; 3**:** e235.

[9] Brinkman RR, Mezei MM, Theilmann J, Almqvist E, Hayden MR. The likelihood of being affected with Huntington disease by a particular age, for a specific CAG size. Am. J. Hum. Genet. 1997; 60: 1202–1210.

[10] Squitieri F,Ciarmiello A,Di Donato S,Frati L. The search for cerebral biomarkers of Huntington's disease: a review of genetic models of age at onset prediction. Eur. J. Neurol. 2006; 13(4): 408-15.

[11] Tabrizi SJ, Langbehn DR, Leavitt BR, Roos RA, Durr A, Craufurd D, Kennard C, Hicks SL, Fox NC et al. Biological and clinical manifestations of Huntington's disease in the longitudinal TRACK-HD study: cross-sectional analysis of baseline data. Lancet Neurol. 2009; 8(9): 791-801.

[12] Tabrizi SJ, Reilmann R, Roos RA, Durr A, Leavitt B, Owen G, Jones R, Johnson H, Craufurd D et al. Potential endpoints for clinical trials in premanifest and early Huntington's disease in the TRACK-HD study: analysis of 24 month observational data. Lancet Neurol. 2012; 1(1): 42–53.

[13] Paulsen JS, Langbehn DR, Stout JC, Aylward E, Ross CA, Nance M, Guttman M, Johnson S, MacDonald M, et al. Detection of Huntington's disease decades before diagnosis: the Predict-HD study. J. Neurol. Neurosurg. Psychiatry 2008, 79(8): 874-80.

[14] Paulsen JS, Nopoulos PC, Aylward E, Ross CA, Johnson H, Magnotta VA, Juhl A, Pierson RK, et al. Striatal and white matter predictors of estimated diagnosis for Huntington disease. Brain Res. Bull. 2010, 82(3-4): 201-7

[15] Tabrizi SJ, Scahill RI, Owen G, Durr A, Leavitt BR, Roos RA, Borowsky B, Landwehrmeyer B et al. Predictors of phenotypic progression and disease onset in premanifest and early-stage Huntington's disease in the TRACK-HD study: analysis of 36-month observational data. Lancet Neurol. 2013, 12: 637–649.

[16] Paulsen JS, Long JD. Onset of Huntington's disease: can it be purely cognitive? Mov. Disord. 2014, 29: 1342–1350.

[17] Epping EA, Kim J, Craufurd D, Brashers-Krug TM, Anderson KE, McCusker E, Luther J, Long JD et al. Longitudinal psychiatric symptoms in prodromal Huntington's disease: a decade of data. Am. J. Psychiatry. 2016, 173(2): 184-92.

[18] Morton AJ, Glynn D, Leavens W, Zheng Z, Faull RL, Skepper JN et al. Paradoxical delay in the onset of disease caused by super-long CAG repeat expansions in R6/2 mice. Neurobiol. Dis. 2009; 33**:** 331-41.

[19] Davies SW, Scherzinger E. Nuclear inclusions in Huntington's disease. Trends Cell Biol. 1997; 7(11): 422.

[20] Dragatsis I, Goldowitz D, Del Mar N, Deng YP, Meade CA, Liu Let al. CAG repeat lengths > or =335 attenuate the phenotype in the R6/2 Huntington's disease transgenic mouse. Neurobiol. Dis. 2009; 33**:** 315-30.

[21] Cummings DM, Alaghband Y, Hickey MA, Joshi PR, Hong SC, Zhu C et al. A critical window of CAG repeat-length correlates with phenotype severity in the R6/2 mouse model of Huntington's disease. J. Neurophysiol. 2012; 107**:** 677-91.

[22] Sawiak SJ, Wood NI, Williams GB, Morton AJ, Carpenter TA. Voxel-based morphometry with templates and validation in a mouse model of Huntington's disease. Magn. Reson. Imaging 2013; 31**:** 1522-31.

[23] Kielar C, Sawiak SJ, Navarro Negredo P, Tse DH, Morton AJ. Tensor-based morphometry and stereology reveal brain pathology in the complexin1 knockout mouse. PLoS One 2012; 7**:** e32636.

[24] Duzdevich D, Li J, Whang J, Takahashi H, Takeyasu K, Dryden DT et al. Unusual structures are present in DNA fragments containing super-long Huntingtin CAG repeats. PLoS One 2011; 6(2): e17119.

[25] Ashburner J. A fast diffeomorphic image registration algorithm. Neuroimage 2007; 38**:** 95-113.

[26] Sawiak SJ, Wood NI, Williams GB, Morton AJ, Carpenter TA. Voxel-based morphometry in the R6/2 transgenic mouse reveals differences between genotypes not seen with manual 2D morphometry. Neurobiol. Dis. 2009b; 33**:** 20-7.

[27] Ashburner J, Friston KJ. Voxel-based morphometry--the methods. Neuroimage 2000; 11**:** 805-21.

[28] Genovese CR, Lazar NA, Nichols T. Thresholding of statistical maps in functional neuroimaging using the false discovery rate. Neuroimage 2002; 15**:** 870-8.

[29] Sawiak SJ, Wood NI, Williams GB, Morton AJ, Carpenter TA. Use of magnetic resonance imaging for anatomical phenotyping of the R6/2 mouse model of Huntington's disease. Neurobiol. Dis. 2009a; 33**:** 12-9.

[30] Provencher SW. Estimation of metabolite concentrations from localized in vivo proton NMR spectra. Magn. Reson. Med. 1993; 30**:** 672-9.

[31] Heikkinen T, Lehtimäki K, Vartiainen N, Puoliväli J, Hendricks SJ, Glaser JR et al. Characterization of neurophysiological and behavioral changes, MRI brain volumetry and 1H MRS in zQ175 knock-in mouse model of Huntington's disease. PLoS One 2012; 7**:** e50717.

[32] Andrew SE, Goldberg YP, Kremer B, Telenius H, Theilmann J, AdamA et al. The relationship between trinucleotide (CAG) repeat length and clinical features of Huntington's disease. Nat. Genet. 1993; 4: 398–403.

[33] Snell RG, MacMillan JC, Cheadle JP, Fenton I, Lazarou LP, Davies P et al. Relationship between trinucleotide repeat expansion and phenotypic variation in Huntington's disease. Nat. Genet. 1993; 4: 393–397.

[34] Lione LA, Carter RJ, Hunt MJ, Bates GP, Morton AJ, Dunnett SB. Selective discrimination learning impairments in mice expressing the human Huntington's disease mutation. J. Neurosci. 1999; 19(23): 10428-37.

[35] Rattray I, Smith E, Gale R, Matsumoto K, Bates GP, Modo M. Correlations of behavioral deficits with brain pathology assessed through longitudinal MRI and histopathology in the R6/2 mouse model of HD. PLoS One. 2013, 8(4): e60012.

[36] Molero AE, Gokhan S, Gonzalez S, Feig JL, Alexandre LC, Mehler MF. Impairment of developmental stem cell-mediated striatal neurogenesis and pluripotency genes in a knock-in model of Huntington's disease. Proc. Natl. Acad. Sci. USA 2009; 106(51): 21900-5.

[37] Molero AE, Arteaga-Bracho EE, Chen CH, Gulinello M, Winchester ML, Pichamoorthy N et al. Selective expression of mutant huntingtin during development recapitulates characteristic features of Huntington's disease. Proc. Natl. Acad. Sci. USA 2016; 113(20): 5736-41.

[38] Sturrock A, Laule C, Decolongon J, Dar Santos R, Coleman AJ, Creighton S. et al. Magnetic resonance spectroscopy biomarkers in premanifest and early Huntington disease. Neurology 2010; 75(19): 1702-1710.

[39] Sturrock A, Laule C, Wyper K, Milner RA, Decolongon J, Dar Santos R et al. A longitudinal study of magnetic resonance spectroscopy Huntington's disease biomarkers. Mov. Disord. 2015; 30(3): 393-401.

[40] van den Bogaard SJ, Dumas EM, Teeuwisse WM, Kan HE, Webb A, van Buchem MA et al. Longitudinal metabolite changes in Huntington's disease during disease onset. J. Huntington's Dis. 2014; 3(4): 377-386.

[41] Jenkins BG, Klivenyi P, Kustermann E, Andreassen OA, Ferrante RJ, Rosen BR et al. Nonlinear decrease over time in N-acetyl aspartate levels in the absence of neuronal loss and increases in glutamine and glucose in transgenic Huntington's disease mice. J. Neurochem. 2012; 74(5):2108-19.

[42] Tkac I, Dubinsky JM, Keene CD, Gruetter R, Low WC.Neurochemical changes in Huntington R6/2 mouse striatum detected by in vivo 1H NMR spectroscopy. J. Neurochem. 2007; 100**:** 1397-406.

[43] Moffett JR, Ross B, Arun P, Madhavarao CN, Namboodiri AM. N-Acetylaspartate in the CNS: from neurodiagnostics to neurobiology. Prog. Neurobiol. 2007; 81(2): 89-131.

[44] van den Bogaard SJ, Dumas EM, Teeuwisse WM, Kan HE, Webb A, Roos RA et al. Exploratory 7-Tesla magnetic resonance spectroscopy in Huntington's disease provides in vivo evidence for impaired energy metabolism. J. Neurol. 2011; 258(12): 2230-2239.

[45] Padowski JM, Weaver KE, Richards TL, Laurino MY, Samii A, Aylward EH et al. Neurochemical correlates of caudate atrophy in Huntington's disease. Mov. Disord. 2014; 29(3): 327-335.

[46] Reynolds GP, Pearson SJ. Decreased glutamic acid and increased 5-hydroxytryptamine in Huntington's disease brain. Neurosci. Lett. 1987; 78: 233-238.

[47] Young AB, Greenamyre JT, Hollingsworth Z, Albin R, D'Amato C, Shoulson I et al. NMDA receptor losses in putamen from patients with Huntington's disease. Science 1988; 241: 981-983.

[48] Dedeoglu A, Choi JK, Cormier K, Kowall NW, Jenkins BG. Magnetic resonance spectroscopic analysis of Alzheimer's disease mouse brain that express mutant human APP shows altered neurochemical profile. Brain Res. 2004; 1012**:** 60-5.

[49] Rivas-Arancibia S, Rodríguez AI, Zigova T, Willing AE, Brown WD, Cahill DW et al. Taurine increases rat survival and reduces striatal damage caused by 3-nitropropionic acid. Int. J. Neurosci. 2001; 108**:** 55-67.

[50] Opstad KS, Bell BA, Griffiths JR, Howe FA. Taurine: a potential marker of apoptosis in gliomas. Br. J. Cancer 2009; 100**:** 789-94.

[51] Law RO. Regulation of mammalian brain cell volume. J. Exp. Zool. 1994a; 268**:** 90-6.

[52] Law RO. Taurine efflux and the regulation of cell volume in incubated slices of rat cerebral cortex. Biochim. Biophys. Acta 1994b; 1221**:** 21-8.

[53] Tsang TM, Woodman B, McLoughlin GA, Griffin JL, Tabrizi SJ, Bates GP et al. Metabolic characterization of the R6/2 transgenic mouse model of Huntington's disease by high-resolution MAS 1H NMR spectroscopy. J. Proteome Res. 2006; 5**:** 483-92.

[54] Gomez-Anson B, Alegret M, Munoz E, Sainz A, Monte GC,Tolosa E. Decreased frontal choline and neuropsychologicalperformance in preclinical Huntington disease. Neurology 2007; 68(12): 906-910.

[55] Ashburner J, Friston KJ. Unified segmentation. Neuroimage 2005; 26**:** 839-51.

Figure legends

Figure 1. Sagittal, coronal and horizontal MR images comparing examples of WT mice at 40 weeks (A-C), R6/2 CAG 250 mice at 25 weeks (D-F), and R6/2 CAG 350 mice at 32 weeks (G-I). At the end stage of their disease there is pronounced atrophy in the cortex of 250 CAG mice (arrows), and in the caudate of 250 and 350 CAG mice, leading to enlarged ventricles (asterisks). White lines indicate the relative positions of the three slices.

Figure 2. Serial coronal slices from R6/2 250 CAG repeat mice (A) and 350 CAG repeat mice (B) at 12-15 weeks of age, showing TBM comparisons of local volume relative to WT mice. Statistical colour map of brain atrophy of slices from age-matched R6/2 mice shows that atrophy is more severe in mice with 250 CAG repeats than it is in mice with 350 CAG repeats. Slices are 400μm apart, and are orientated from anterior (top left) to posterior (bottom right). The colour bar shows Student's *t*-score with 24 degrees of freedom.

Figure 3. Serial coronal slices from R6/2 250 CAG and 350 CAG repeat mice, showing average volume differences relative to WT mice over time. Progression of atrophy is slower in 350 CAG repeat mice, and less pronounced at end-stage in 350 CAG mice than it is in 250 CAG repeat mice. Note that equivalent levels of atrophy take around 10 weeks longer to appear in 350 CAG than 250 CAG mice (for example, compare changes at 18-21 weeks in 350 CAG mice with that at 8-12 weeks in 250 CAG mice).

Figure 4. Serial coronal slices from R6/2 250 CAG repeat mice (A-D) and 350 CAG repeat mice (E-H) at 12-15 weeks of age, showing layering of cortical

atrophy. Slices from Figure 2 shown at higher magnification demonstrate that in the more caudal aspects of the cortex in R6/2 250 CAG repeat mice in particular, deeper layers show greater atrophy than the superficial layers (C-D). Atrophy in the cortex of 350 CAG mice at 12-15 weeks is confined to deep layers (E-F).

Figure 5. **Progression of volume change in selected regional brain areas with age in WT and R6/2 mice.** Data points are volumes of cortex (A), caudate putamen (B), lateral ventricles (C), amygdaloid nucleus (D), hippocampal formation (E), internal capsule (F) and cerebellum (G) for all individual mice. Solid lines show robust fits to the data with shaded regions indicating one standard deviation above and below the line respectively. Black lines = WT mice; red lines = R6/2 250 CAG mice; blue lines = R6/2 350 CAG mice.

Figure 6. Metabolite concentrations (relative to overall creatine + phosphocreatine levels), in striatum of WT and R6/2 mice. Data points show relative concentrations of aspartate (A), choline (B), glutamine and glutamate (C) and taurine (D) from individual mice. Solid lines show robust fits to the data with shaded regions indicating one standard deviation above and below the line respectively. Black lines: = WT mice; red lines = R6/2 250 CAG mice; blue lines = R6/2 350 CAG mice.

Supplementary Figure 1. Sex difference in rate of volume change in the lateral ventricles with age in WT and R6/2 mice. Solid lines show robust fits to the data with shaded regions indicating one standard deviation above and below the line respectively. Black lines = WT mice; red lines = R6/2 250 CAG mice; blue lines = R6/2 350 CAG mice. Left panel, male mice; right panel, female mice.

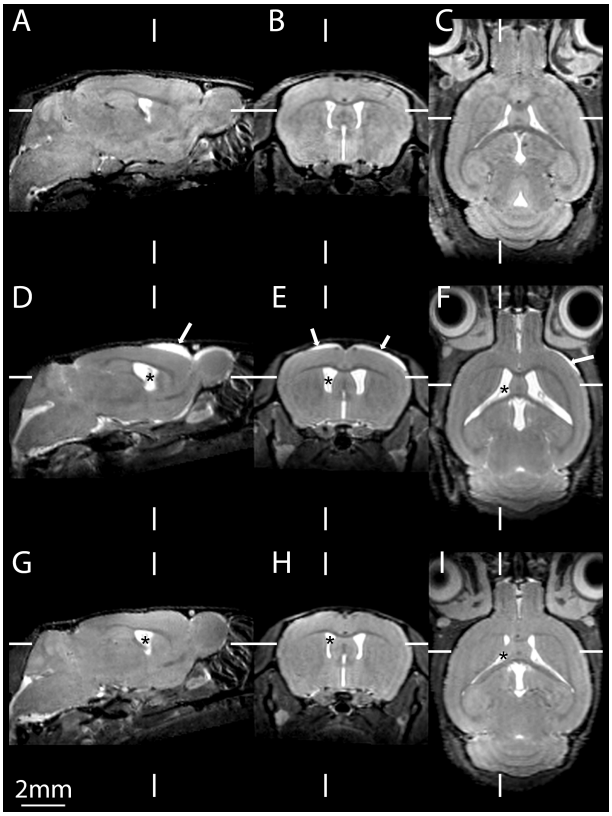

Figure 1

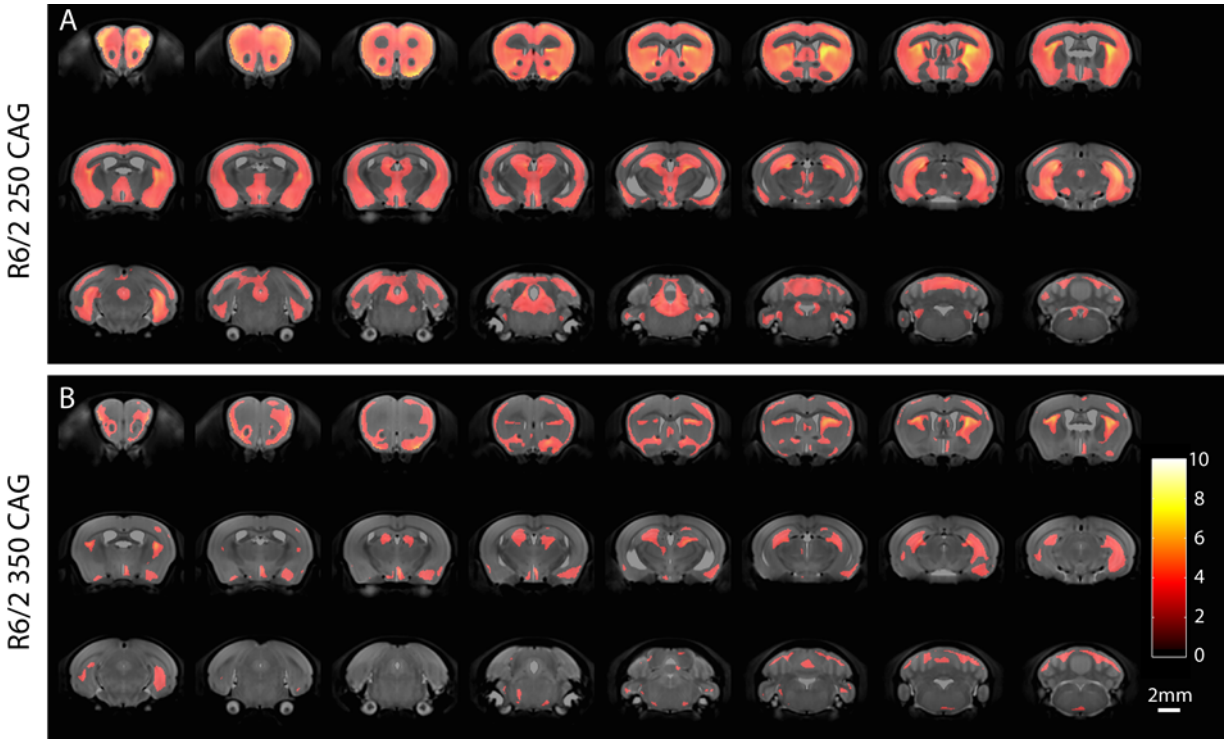

Figure 2

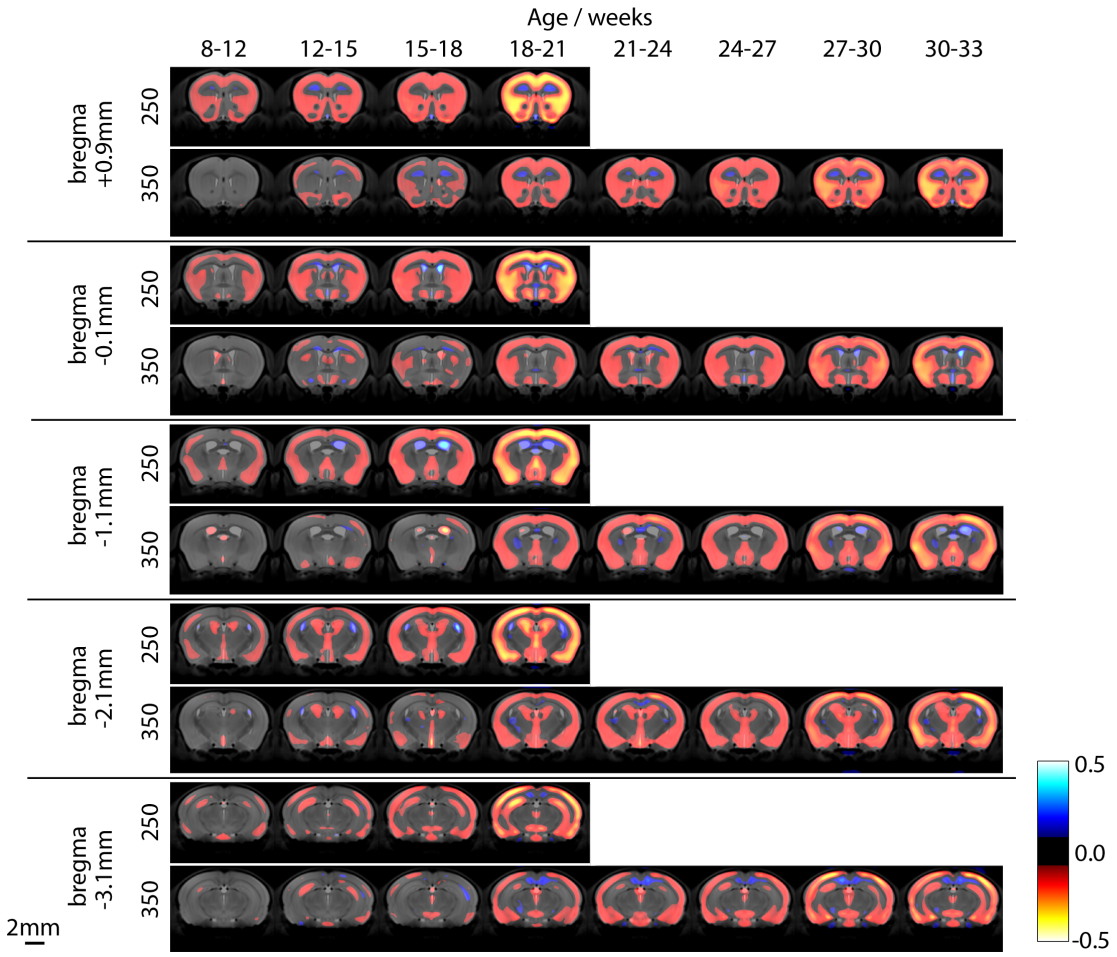
Age / weeks
8-12
12-15
15-18
18-21
21-24
24-27
27-30
30-33
bregma +0.9mm
bregma -0.1mm
bregma -1.1mm
bregma -2.1mm
bregma -3.1mm
250
350
2mm
0.5
0.0
-0.5

Figure 3

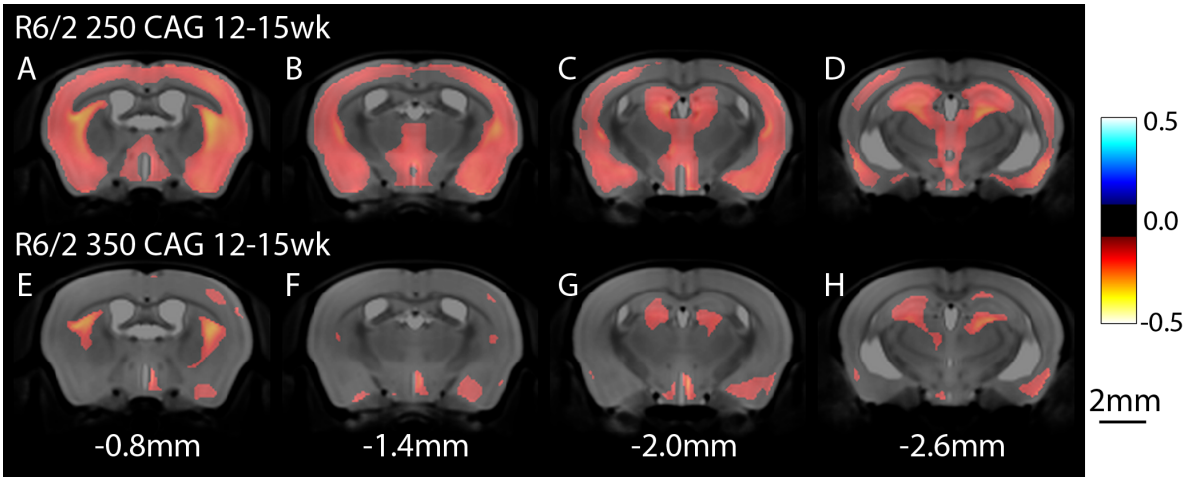
R6/2 250 CAG 12-15wk
A
B
C
D
R6/2 350 CAG 12-15wk
E
F
G
H
0.5
0.0
-0.5
2mm
-0.8mm
-1.4mm
-2.0mm
-2.6mm

Figure 4

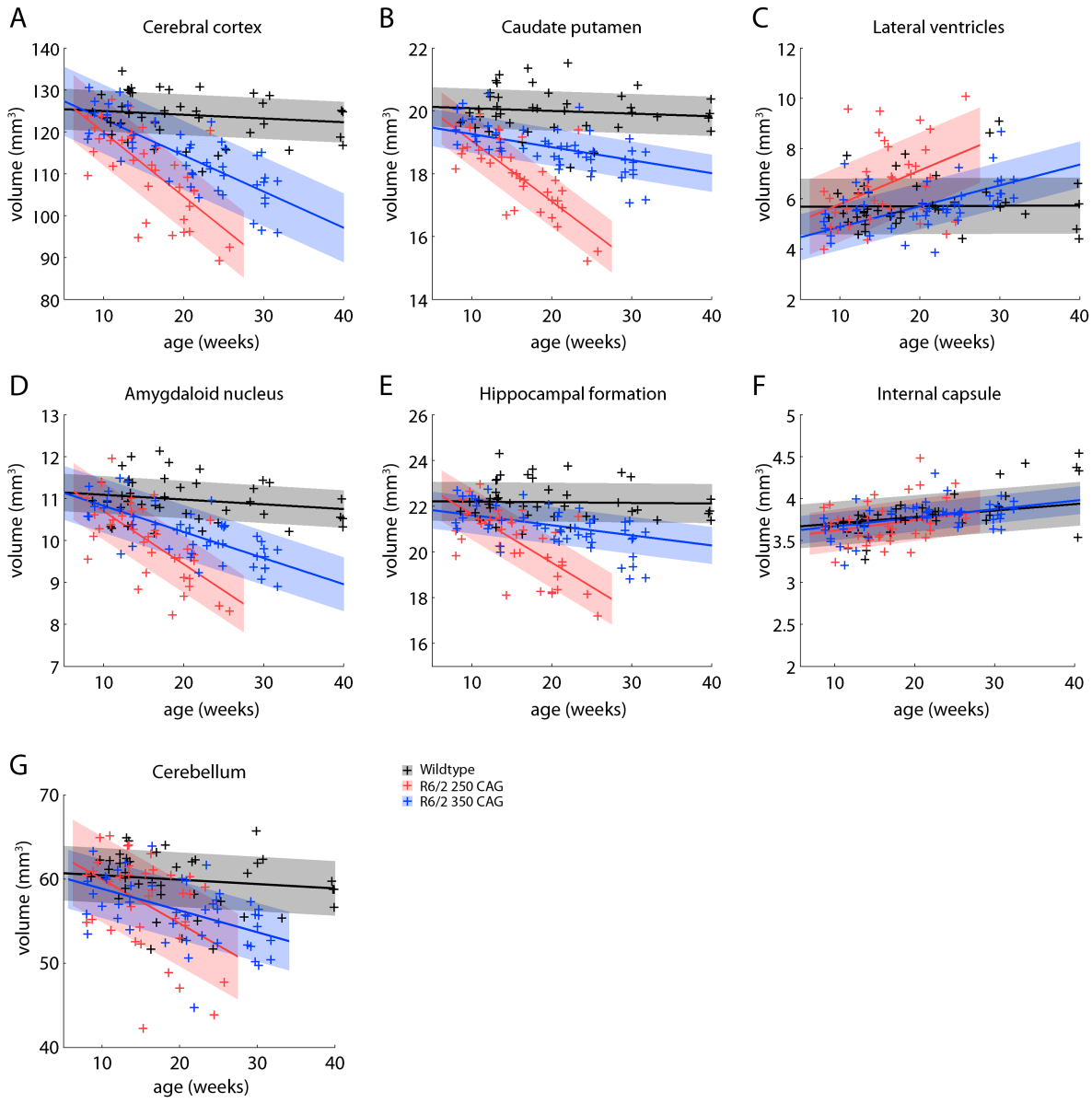
A
Cerebral cortex
volume (mm³)
age (weeks)
B
Caudate putamen
volume (mm³)
age (weeks)
C
Lateral ventricles
volume (mm³)
age (weeks)
D
Amygdaloid nucleus
volume (mm³)
age (weeks)
E
Hippocampal formation
volume (mm³)
age (weeks)
F
Internal capsule
volume (mm³)
age (weeks)
G
Cerebellum
volume (mm³)
age (weeks)
Wildtype
R6/2 250 CAG
R6/2 350 CAG

Figure 5

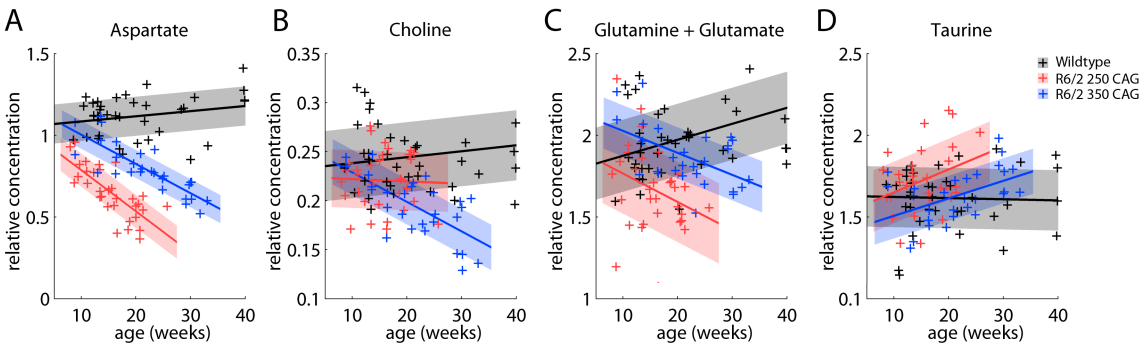
A
Aspartate
B
Choline
C
Glutamine + Glutamate
D
Taurine
relative concentration
age (weeks)
Wildtype
R6/2 250 CAG
R6/2 350 CAG

Figure 6

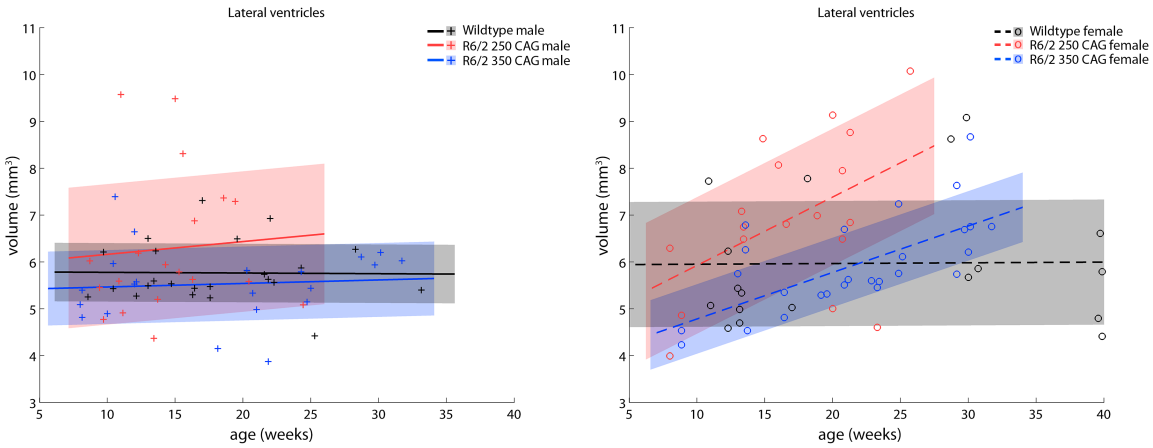

Supplementary Figure 1